INTERNATIONAL JOURNAL FOR NUMERICAL METHODS IN FLUIDS
Int. J. Numer. Meth. Fluids 2004; **44**:463–482 (DOI: 10.1002/fld.647)

An upwind compact approach with group velocity control for compressible flow fields

Qingyong Zhu[1,2,*,†] and Yi Li[2]

[1]*School of Mathematics and Computational Science, Zhongshan University, Guangzhou, China*
[2]*The Hong Kong Polytechnic University, Hung Hom, Kowloon, Hong Kong, China*

SUMMARY

In this paper we construct an upwind compact finite difference scheme with group velocity control for better simulation of compressible flow fields. Compared with traditional difference schemes, compact schemes have higher accuracy for the same stencil width. By means of the characteristic analysis of the operators, the group velocity of wave packets will be controlled to suppress the non-physical oscillations in numerical solutions. In numerical simulation of the 3D compressible flow fields the third-order accurate upwind compact operator is used to approximate the derivatives in the convection terms of the compressible N–S equations, the traditional finite difference scheme is used to approximate the viscous terms. Numerical solutions indicate that the method is satisfactory. Copyright © 2004 John Wiley & Sons, Ltd.

KEY WORDS: upwind compact finite difference method; group velocity control; shock capture technique; non-physical oscillations; TVB property; compressible flow fields

1. INTRODUCTION

In recent years, a number of high-order accurate finite difference schemes have been developed for better simulation of the complex flow fields. The key point for correctly simulating the complex flow fields with a range of scales is that the method can capture well the vortices with small scales and shocks. Traditional second-order total variation diminishing (TVD) schemes have high resolution of the shocks. However, there are some undesirable defects. First, these schemes drop to first-order spatial accuracy at local extreme. Next, when it is

*Correspondence to: Qingyong Zhu, School of Mathematics and Computational Science, Zhongshan University, 510275 Guangzhou, People's Republic of China.
†E-mail: qingyongzhu@yahoo.com

Contract/grant sponsor: National Natural Science Foundation of China; contract/grant number: 10102024
Contract/grant sponsor: Hong Kong Polytechnic University

Received 9 November 2002
Revised 17 May 2003

used to solve the viscous flows especially to solve the problem at high Reynolds number, the numerical dissipation may exceed the physical dissipation. It leads to unsatisfactory results. Fu and Ma [1] pointed out that the restriction on the mesh Reynolds number can be relaxed with higher accurate schemes. Therefore, it is necessary to develop high-order accurate finite difference schemes. For the traditional two-level explicit schemes, we have to use at least $(N+1)$ nodes to achieve Nth-order accuracy. When N is large, the stencil is surprisingly wide, thus neither compact nor efficient. Furthermore, the treatment of boundary is also difficult. Consequently the number of numerical boundary conditions is increased. Meanwhile many existing schemes with high resolution of the shock are complicated and expensive. Due to two attractive features of the compact schemes and upwind compact schemes: high-order accuracy and small stencil, these schemes become popular in CFD area. Compact schemes are methods where the derivatives are approximated not by polynomial operators but by rational function operators on the discrete solutions.

In previous papers, Leonard [2] suggested using a third-order upwind difference for the convection term in the hyperbolic equations. In Reference [3], Rai and Moin presented simulations of a turbulent channel flow by using a high-order upwind biased finite difference scheme. Ma and Fu [4] developed a high-order accurate upwind compact scheme, which has been successfully used to simulate the compressible mixing layers. In 1992, Lele [5] investigated the compact finite difference schemes with spectral-like resolution and simulated the mixing layer with the schemes. In 1996, E and Liu [6] used the compact schemes to simulate the incompressible flow. The computed results are satisfactory. In 1998, Zhu and Ma [7] developed an upwind compact scheme to solve the hyperbolic conservation laws. Chu and Fan [8] studied a three-point combined compact difference scheme. The major features of this scheme are: three point, implicit, sixth-order accuracy, and inclusion of boundary values. Due to its combination of the first and second derivatives, the scheme becomes more compact and more accurate than normal compact difference schemes. In [9] Yabe *et al*. presented a universal solver for hyperbolic equations by introducing a function interpolated by a cubic polynomial between two end points. They introduced a review of the constrained interpolation profile (CIP) method for solid, liquid, gas and plasma. This method has a compact support and sub-cell resolution, including a front-capturing algorithm with functional transformation, a pressure-based algorithm and other miscellaneous physics such as the elastic-plastic effect and surface tension. In these two methods, only two grids are necessary for the 3rd order and three grids for the 5th order. However, these schemes are very complicated and expensive.

The purpose of this paper is to develop a simple and effective numerical method for better simulation of the complex flow fields with shock waves. The reason of oscillation production in numerical solutions is because of non-uniform group velocity of wave packets. In order to improve the shock resolutions we propose a high-order accurate upwind compact finite difference scheme with group velocity control. We follow the TVD ideas and try to control the group velocity of wave packets to avoid spurious oscillations while keeping the formal accuracy of the scheme. Notice that the compact scheme is global due to the tri-diagonal inversion. By means of the idea of a local mean we construct an upwind compact scheme with group velocity control to calculate the discontinuities. The scheme can keep the third-order accuracy in smooth regions. The implicit time discretization is used in this investigation. The characteristic analysis of the operators is given in Section 2. The upwind compact operator with group velocity control (UCGVC3) is analysed in Section 3; The applications of the methods to approximate the N–S equations are presented in Section 4, some numerical examples and

computed results of the model equations are given in Sections 5. The numerical simulations of compressible flow fields are given in Section 6.

2. CHARACTERISTIC ANALYSIS OF OPERATORS

Consider the one-dimensional unsteady advection of scalar u with constant positive velocity a.

$$u_t + au_x = 0 \tag{1}$$

The solution with the initial condition $u(x,0) = u_0(x)$ is $u(x,t) = u_0(x - at)$.

To facilitate the discussion, let L denote the approximate operator of the spatial differential operator $\mathrm{d}/\mathrm{d}x$. $h^{-1} \cdot L \approx \mathrm{d}/\mathrm{d}x$. Analyse the following equation,

$$v_t + (a/h)Lv = 0 \tag{2}$$

Here the same initial condition is used. Making a Fourier transform about variable x, we get

$$\hat{v}_t = -\frac{a}{h}\hat{L}\hat{v} \tag{3}$$

where $\hat{L}(\xi) \in C$ is the symbol of L.

Definition 2.1 (*Dexun Fu and Yanwen Ma* [*10*])
The operator L with $a \cdot \mathrm{Re}[\hat{L}(\xi)] \geqslant 0$, $\forall |\xi| \leqslant \pi$ is dissipative, and with $a \cdot \mathrm{Re}[\hat{L}(\xi)] \equiv 0$, $\forall |\xi| \leqslant \pi$ it is non-dissipative. Let $\mathscr{L}_\mathrm{d}$ denote the set of dissipative operators. $\mathscr{L}_\mathrm{n}$ denotes the set of non-dissipative ones.

Definition 2.2 (*Dexun Fu and Yanwen Ma* [*10*])
The operator L with $\mathrm{d}\,\mathrm{Im}[\hat{L}(\xi)]/\mathrm{d}\xi \leqslant 1$, $\forall |\xi| \leqslant \pi$ is a slow operator. Let $\mathscr{L}_\mathrm{s}$ denote the set of slow operators. The operator L with $\mathrm{d}\,\mathrm{Im}[\hat{L}(\xi)]/\mathrm{d}\xi \geqslant 1$, $\forall |\xi| \leqslant \pi$ is a fast operator. $\mathscr{L}_\mathrm{f}$ denotes the set of fast operators. If $\exists \pi > \xi_0 > 0$, The operator L with $\mathrm{d}\,\mathrm{Im}[\hat{L}(\xi)]/\mathrm{d}\xi \geqslant 1$, $\forall |\xi| \leqslant \xi_0$ and $\mathrm{d}\,\mathrm{Im}[\hat{L}(\xi)]/\mathrm{d}\xi \leqslant 1$, $\forall \xi \in [-\pi, -\xi_0] \cup [\xi_0, \pi]$ is a mixed operator. $\mathscr{L}_\mathrm{m}$ denotes the set of mixed operators.

In approximate solutions non-linear dependence of $\mathrm{Im}[\hat{L}(\xi)]$ on ξ leads to non-uniform group velocity of wave packets. The reason of oscillation production in approximate solutions is non-uniform group velocity of wave packets. In order to prevent the non-physical oscillations in the vicinity of the discontinuities the group velocity of wave packets must be controlled. Therefore, the operator L must satisfy the following conditions:

I: Behind the discontinuity, $L \in \mathscr{L}_\mathrm{f} \cap (\mathscr{L}_\mathrm{d} \cup \mathscr{L}_\mathrm{n})$ or $L \in \mathscr{L}_\mathrm{m} \cap \mathscr{L}_\mathrm{d}$;
II: In front of the discontinuity, $L \in \mathscr{L}_\mathrm{s} \cap (\mathscr{L}_\mathrm{d} \cup \mathscr{L}_\mathrm{n})$.

Given $v(x)$, $x \in R^1$ and a positive parameter $h > 0$. E_h is a shift operator such that $(E_h v)(x) = v(x + h)$. The operators of δ_x^+, δ_x^-, δ_x^0, δ_x^2 are defined as

$$\delta_x^+ := E_h - I, \quad \delta_x^- := I - E_h^{-1}, \quad \delta_x^0 := \tfrac{1}{2}(\delta_x^+ + \delta_x^-), \quad \delta_x^2 := \delta_x^+ \delta_x^- = \delta_x^- \delta_x^+ \tag{4}$$

Here I is an identity operator. The subscript x indicates that the operator is applied in the x direction.

The symbols of the operators δ_x^+, δ_x^-, δ_x^0, δ_x^2 are

$$\hat{\delta}_x^+ = \cos\xi - 1 + \mathrm{i}\sin\xi, \quad \hat{\delta}_x^- = 1 - \cos\xi + \mathrm{i}\sin\xi$$

$$\hat{\delta}_x^0 = \tfrac{1}{2}(\hat{\delta}_x^+ + \hat{\delta}_x^-) = \mathrm{i}\sin\xi, \quad \hat{\delta}_x^2 = \hat{\delta}_x^+\hat{\delta}_x^- = 2\cos\xi - 2$$

where $-\pi \leqslant \xi \leqslant \pi$, $\mathrm{i}^2 = -1$. It is easy to prove the above facts.

Theorem 2.3
If $\sigma > 1/6$, $L = \delta_x^0 - \sigma\delta_x^0\delta_x^2 + 0.5\sigma\delta_x^2\delta_x^2$ is a mixed operator, $L \in \mathscr{L}_\mathrm{m} \cap \mathscr{L}_\mathrm{d}$.

Proof
Making a Fourier transform, we get the symbol of L.

$$\hat{L} = \hat{\delta}_x^0 - \sigma\hat{\delta}_x^0\hat{\delta}_x^2 + 0.5\sigma\hat{\delta}_x^2\hat{\delta}_x^2 = \mathrm{i}\sin\xi - \mathrm{i}\sigma\sin\xi(2\cos\xi - 2) + 0.5\sigma(2\cos\xi - 2)^2$$

$$= 2\sigma(\cos\xi - 1)^2 + \mathrm{i}(\sin\xi + 2\sigma\sin\xi - 2\sigma\cos\xi\sin\xi)$$

In terms of the Definition 2.2, if $4\sigma\cos^2\xi - (1 + 2\sigma)\cos\xi - 2\sigma + 1 \leqslant 0$, $\mathrm{d}\,\mathrm{Im}\lfloor\hat{L}(\xi)\rfloor/\mathrm{d}\xi \geqslant 1$. If $\sigma > 1/6$, $\exists\xi_0 = \arccos((1/4\sigma) - \frac{1}{2})$, when $|\xi| \leqslant \xi_0$, we have

$$\mathrm{d}\,\mathrm{Im}[\hat{L}(\xi)]/\mathrm{d}\xi \geqslant 1. \quad -\pi \leqslant \xi \leqslant -\xi_0 \text{ or } \xi_0 \leqslant \xi \leqslant \pi,$$

$$\mathrm{d}\,\mathrm{Im}[\hat{L}(\xi)]/\mathrm{d}\xi \leqslant 1. \text{ Hence } L \in \mathscr{L}_\mathrm{m}.$$

On the other hand, $a \cdot \mathrm{Re}[\hat{L}(\xi)] = 2a \cdot \sigma(\cos\xi - 1)^2 \geqslant 0$, $\forall|\xi| \leqslant \pi$ implies $L \in \mathscr{L}_\mathrm{d}$. Therefore, if $\sigma > \frac{1}{6}$, $L \in \mathscr{L}_\mathrm{m} \cap \mathscr{L}_\mathrm{d}$. □

Similar to Theorem 2.3, we have the following theorem.

Theorem 2.4
$L = \delta_x^0 + \sigma\delta_x^0\delta_x^2 + 0.5\sigma\delta_x^2\delta_x^2$, $\frac{1}{2} \geqslant \sigma \geqslant 0$ is a slow operator, $L \in \mathscr{L}_\mathrm{s} \cap (\mathscr{L}_\mathrm{d} \cup \mathscr{L}_\mathrm{n})$.

Proof
The proof is similar to the above theorem and is thus omitted. □

The stencils of the operator L can be expressed as

$$\underset{}{\overset{a > 0}{\longrightarrow}}$$

$j-2$	$j-1$	j	$j+1$	$j+2$
×	×	⊗	×	

Behind the discountinuity, $L = \delta_x^0 - \sigma\delta_x^0\delta_x^2 + 0.5\sigma\delta_x^2\delta_x^2, \sigma > \frac{1}{6}$

	×	⊗	×	×

In front of the discountinuity, $L = \delta_x^0 + \sigma\delta_x^0\delta_x^2 + 0.5\sigma\delta_x^2\delta_x^2, \frac{1}{2} \geqslant \sigma \geqslant 0$

Given $v_j = v(jh)$, $j \in Z$, we have

$$(1/h)(\delta_x^0 - \sigma\delta_x^0\delta_x^2 + 0.5\sigma\delta_x^2\delta_x^2)v_j = (1/h)\left[\sigma v_{j-2} - \left(\tfrac{1}{2} + 3\sigma\right) v_{j-1} + 3\sigma v_j + \left(\tfrac{1}{2} - \sigma\right) v_{j+1}\right] \quad (5)$$

where $\sigma > \frac{1}{6}$. If $\sigma = \frac{1}{2}$, we get the three-node second-order accurate upwind operator $(1/h)L(v_j) = (1/2h)(v_{j-2} - 4v_{j-1} + 3v_j)$

$$(1/h)(\delta_x^0 + \sigma\delta_x^0\delta_x^2 + 0.5\sigma\delta_x^2\delta_x^2)v_j = (1/h)\left[-\left(\tfrac{1}{2} + \sigma\right) v_{j-1} + 3\sigma v_j + \left(\tfrac{1}{2} - 3\sigma\right) v_{j+1} + \sigma v_{j+2}\right] \quad (6)$$

where $\frac{1}{2} \geqslant \sigma \geqslant 0$. If $\sigma = 0$, we get the central difference operator $(1/h)L(v_j) = (1/2h)(v_{j+1} - v_{j-1})$.

We can see that the mixed operators $(1/h)L = (1/h)(\delta_x^0 - \sigma\delta_x^0\delta_x^2 + 0.5\sigma\delta_x^2\delta_x^2)$, $\sigma > \frac{1}{6}$ and the slow operators $(1/h)L = (1/h)(\delta_x^0 + \sigma\delta_x^0\delta_x^2 + 0.5\sigma\delta_x^2\delta_x^2)$, $\frac{1}{2} \geqslant \sigma \geqslant 0$ are second-order accurate biased difference operators. They occupy the nodes of $(j-2, j-1, j, j+1)$ and $(j-1, j, j+1, j+2)$, respectively. Actually TVD scheme is a kind of adaptable methods, the three-node second-order accurate upwind operator, $(1/h)L(v_j) = (1/2h)(v_{j-2} - 4v_{j-1} + 3v_j)$ is employed behind the shock, in front of the shock the central difference operator $(1/h)L(v_j) = (1/2h)(v_{j+1} - v_{j-1})$ is used. It is implemented by a minmod function. We follow this idea and construct an upwind compact method with group velocity control. This method satisfies the TVB property. The mean $\bar{v}_j := Av_j = (\frac{1}{6} + \varepsilon)v_{j-1} + \frac{2}{3}v_j + (\frac{1}{6} - \varepsilon)v_{j+1}$ of v_j is used to replace v_j. Here A is a $N \times N$ matrix. The above-mentioned operators are applied on $\bar{v}_j$. Under appropriate conditions $\mathrm{TV}(\bar{v})$ is diminishing. A recovery from $\bar{v}_j$ to v_j is needed. If the transpose of A is strongly diagonally dominant, we will see that $\mathrm{TV}(v)$ is bounded.

3. THIRD-ORDER ACCURATE UPWIND COMPACT OPERATOR WITH GROUP VELOCITY CONTROL (UCGVC3)

3.1. One-space dimension

For the conservation form,

$$\begin{aligned} u_t + f(u)_x &= 0 \\ u(x,0) &= u_0(x) \end{aligned} \quad (7)$$

Consider the semi-discrete form, a compact scheme for solving the equation can be expressed as

$$\frac{\mathrm{d}u_j}{\mathrm{d}t} = -\frac{1}{h}(A^{-1}Bf(u))_j \equiv L(u)_j \quad (8)$$

where A, B are both local operators. The tri-diagonal inversion A^{-1} is not local. Here $A = I - 2\varepsilon\delta_x^0 + \frac{1}{6}\delta_x^2$, $B = \delta_x^0 - 2\varepsilon\delta_x^2$, $(-\frac{1}{3} < \varepsilon < \frac{1}{3})$. We define

$$\bar{u}_j := Au_j = \left(\tfrac{1}{6} + \varepsilon\right) u_{j-1} + \tfrac{2}{3}\, u_j + \left(\tfrac{1}{6} - \varepsilon\right) u_{j+1} \quad (9a)$$

$$Bu_j = \left(\tfrac{1}{2} - 2\varepsilon\right) u_{j+1} + 4\varepsilon u_j - (\tfrac{1}{2} + 2\varepsilon)u_{j-1} \quad (9b)$$

The scheme (8) can be expressed as

$$\frac{\mathrm{d}\bar{u}_j}{\mathrm{d}t} = -\frac{1}{h}(\delta_x^0 - 2\varepsilon\delta_x^2) f(u)_j \tag{10}$$

To avoid spurious oscillations while keeping the formal accuracy of the scheme we employ a switching function 'φ_j' [11],

$$\varphi_j = \begin{cases} 1, & \dfrac{|u_{j+1} - 2u_j + u_{j-1}|}{0.5(|u_{j+1} - u_j| + |u_j - u_{j-1}|) + 0.5|u_{j+1} + 2u_j + u_{j-1}|} \geqslant \kappa \\ 0, & \dfrac{|u_{j+1} - 2u_j + u_{j-1}|}{0.5(|u_{j+1} - u_j| + |u_j - u_{j-1}|) + 0.5|u_{j+1} + 2u_j + u_{j-1}|} < \kappa \end{cases} \tag{11}$$

where κ is a threshold. $\varphi_j = 1$ in the vicinity of shocks and $\varphi_j = 0$ in smooth regions. The switch function φ_j can guarantee that the obtained scheme is $O(h^3)$ in smooth regions.

In accordance with Theorems 2.3 and 2.4 the upwind compact scheme with group velocity control can be constructed as follows ($\sigma = \frac{1}{2}$),

$$\begin{aligned} \frac{\mathrm{d}\bar{u}_j}{\mathrm{d}t} = & -\frac{1}{h}\delta_x^0[f(u)_j - \varphi_j(f(u)_j - f(\bar{u})_j)] + \frac{1}{2h}\delta_x^0[\varphi_j \cdot ss_j a\delta_x^2\bar{u}_j] - \frac{1}{4h}\delta_x^2[\varphi_j \cdot a\delta_x^2\bar{u}_j] \\ & + \frac{2\varepsilon}{h}\delta_x^2[f(u)_j - \varphi_j(f(u)_j - f(\bar{u})_j)] \end{aligned} \tag{12}$$

where $\varepsilon \cdot f'(u) \geqslant 0$, $-\frac{1}{3} < \varepsilon < \frac{1}{3}$, $a = \max_u |f'(u)|$. $ss_j = \mathrm{sgn}(\delta_x^0\bar{u}_j \cdot \delta_x^2\bar{u}_j)$ is called shock structure function in the present paper. The recovery from $\bar{u}$ to u is needed, $u_j = (I - 2\varepsilon\delta_x^0 + \frac{1}{6}\delta_x^2)^{-1}\bar{u}_j$. This recovery is global.

Theorem 3.1

Semi-discrete Scheme (12) satisfies the TVDM property (total variation bounded in the means) in the vicinity of discontinuities:

$$\frac{\mathrm{d}}{\mathrm{d}t}\mathrm{TV}(\bar{u}) \leqslant 0 \tag{13}$$

Proof

In the vicinity of discontinuities $\varphi_j = 1$, consider the following four cases,

Case 1: $ss_{j+1} = ss_{j-1} = 1$, Semi-discrete form (12) can be rewritten as

$$\begin{aligned} \frac{\mathrm{d}\bar{u}_j}{\mathrm{d}t} &= \frac{1}{h}C_{j+1/2}^+\delta_x^+\bar{u}_j - \frac{1}{h}C_{j-1/2}^-\delta_x^-\bar{u}_j \\ &= \frac{1}{2h}\left(a - \frac{f(\bar{u})_{j+1} - f(\bar{u})_j}{\bar{u}_{j+1} - \bar{u}_j} + 4\varepsilon\frac{f(\bar{u})_{j+1} - f(\bar{u})_j}{\bar{u}_{j+1} - \bar{u}_j}\right)\delta_x^+\bar{u}_j \\ &\quad - \frac{1}{2h}\left[\frac{f(\bar{u})_j - f(\bar{u})_{j-1}}{\bar{u}_j - \bar{u}_{j-1}} + a\left(2 - \frac{\bar{u}_{j-1} - \bar{u}_{j-2}}{\bar{u}_j - \bar{u}_{j-1}}\right) + 4\varepsilon\frac{f(\bar{u})_j - f(\bar{u})_{j-1}}{\bar{u}_j - \bar{u}_{j-1}}\right]\delta_x^-\bar{u}_j \end{aligned} \tag{14}$$

where

$$C^{+,1}_{j+1/2}=\frac{1}{2}\left(a-\frac{f(\bar{u})_{j+1}-f(\bar{u})_j}{\bar{u}_{j+1}-\bar{u}_j}\right),\quad C^{+,2}_{j+1/2}=2\varepsilon\,\frac{f(\bar{u})_{j+1}-f(\bar{u})_j}{\bar{u}_{j+1}-\bar{u}_j}$$

$$C^{-,1}_{j-1/2}=\frac{1}{2}\left[\frac{f(\bar{u})_j-f(\bar{u})_{j-1}}{\bar{u}_j-\bar{u}_{j-1}}+a\left(2-\frac{\bar{u}_{j-1}-\bar{u}_{j-2}}{\bar{u}_j-\bar{u}_{j-1}}\right)\right],\quad C^{-,2}_{j-1/2}=2\varepsilon\,\frac{f(\bar{u})_j-f(\bar{u})_{j-1}}{\bar{u}_j-\bar{u}_{j-1}}$$

Obviously $C^{+,1}_{j+1/2}\geqslant 0$, $C^{+,2}_{j+1/2}\geqslant 0$, $C^{-,2}_{j-1/2}\geqslant 0$.

If $\bar{u}_{j-1}-\bar{u}_{j-2}/\bar{u}_j-\bar{u}_{j-1}\leqslant 0$, $C^{-,1}_{j-1/2}\geqslant 0$.

If $\bar{u}_{j-1}-\bar{u}_{j-2}/\bar{u}_j-\bar{u}_{j-1}>0$, the condition

$$ss_{j-1}=\mathrm{sgn}(\delta^0_x\bar{u}_{j-1}\cdot\delta^2_x\bar{u}_{j-1})\mathrm{sgn}\left[\frac{(\delta^+_x\bar{u}_{j-1})^2-(\delta^-_x\bar{u}_{j-1})^2}{2}\right]=1$$

implies $|\bar{u}_j-\bar{u}_{j-1}|>|\bar{u}_{j-1}-\bar{u}_{j-2}|$. Therefore, $\bar{u}_{j-1}-\bar{u}_{j-2}/\bar{u}_j-\bar{u}_{j-1}<1$,

$$C^{-,1}_{j-1/2}=\frac{1}{2}\left[a+\frac{f(\bar{u})_j-f(\bar{u})_{j-1}}{\bar{u}_j-\bar{u}_{j-1}}+a\left(1-\frac{\bar{u}_{j-1}-\bar{u}_{j-2}}{\bar{u}_j-\bar{u}_{j-1}}\right)\right]\geqslant 0$$

In this case $C^+_{j+1/2}=C^{+,1}_{j+1/2}+C^{+,2}_{j+1/2}\geqslant 0$, $C^-_{j-1/2}=C^{-,1}_{j-1/2}+C^{-,2}_{j-1/2}\geqslant 0$.

Case 2: $ss_{j+1}=ss_{j-1}=-1$, Equation (12) can be rewritten as

$$\begin{aligned}\frac{\mathrm{d}\bar{u}_j}{\mathrm{d}t}&=\frac{1}{h}C^+_{j+1/2}\delta^+_x\bar{u}_j-\frac{1}{h}C^-_{j-1/2}\delta^-_x\bar{u}_j\\&=\frac{1}{2h}\left[-\frac{f(\bar{u})_{j+1}-f(\bar{u})_j}{\bar{u}_{j+1}-\bar{u}_j}+a\left(2-\frac{\bar{u}_{j+2}-\bar{u}_{j+1}}{\bar{u}_{j+1}-\bar{u}_j}\right)+4\varepsilon\,\frac{f(\bar{u})_{j+1}-f(\bar{u})_j}{\bar{u}_{j+1}-\bar{u}_j}\right]\delta^+_x\bar{u}_j\\&\quad-\frac{1}{2h}\left[\frac{f(\bar{u})_j-f(\bar{u})_{j-1}}{\bar{u}_j-\bar{u}_{j-1}}+a+4\varepsilon\,\frac{f(\bar{u})_j-f(\bar{u})_{j-1}}{\bar{u}_j-\bar{u}_{j-1}}\right]\delta^-_x\bar{u}_j\end{aligned}\tag{15}$$

where

$$C^{+,1}_{j+1/2}=\frac{1}{2}\left[-\frac{f(\bar{u})_{j+1}-f(\bar{u})_j}{\bar{u}_{j+1}-\bar{u}_j}+a\left(2-\frac{\bar{u}_{j+2}-\bar{u}_{j+1}}{\bar{u}_{j+1}-\bar{u}_j}\right)\right],\quad C^{+,2}_{j+1/2}=2\varepsilon\,\frac{f(\bar{u})_{j+1}-f(\bar{u})_j}{\bar{u}_{j+1}-\bar{u}_j}$$

$$C^{-,1}_{j-1/2}=\frac{1}{2}\left(\frac{f(\bar{u})_j-f(\bar{u})_{j-1}}{\bar{u}_j-\bar{u}_{j-1}}+a\right),\quad C^{-,2}_{j-1/2}=2\varepsilon\,\frac{f(\bar{u})_j-f(\bar{u})_{j-1}}{\bar{u}_j-\bar{u}_{j-1}}$$

Obviously $C^{-,1}_{j-1/2}\geqslant 0$, $C^{-,2}_{j-1/2}\geqslant 0$, $C^{+,2}_{j+1/2}\geqslant 0$.

If $\bar{u}_{j+2}-\bar{u}_{j+1}/\bar{u}_{j+1}-\bar{u}_j\leqslant 0$, $C^{+,1}_{j+1/2}\geqslant 0$.

If $\bar{u}_{j+2}-\bar{u}_{j+1}/\bar{u}_{j+1}-\bar{u}_j>0$, the condition $ss_{j+1}=\mathrm{sgn}(\delta^0_x\bar{u}_{j+1}\cdot\delta^2_x\bar{u}_{j+1})=-1$ implies $|\bar{u}_{j+2}-\bar{u}_{j+1}|<|\bar{u}_{j+1}-\bar{u}_j|$. Therefore, $\bar{u}_{j+2}-\bar{u}_{j+1}/\bar{u}_{j+1}-\bar{u}_j<1$,

$$C^{+,1}_{j+1/2}=\frac{1}{2}\left[a-\frac{f(\bar{u})_{j+1}-f(\bar{u})_j}{\bar{u}_{j+1}-\bar{u}_j}+a\left(1-\frac{\bar{u}_{j+2}-\bar{u}_{j+1}}{\bar{u}_{j+1}-\bar{u}_j}\right)\right]\geqslant 0$$

In this case $C^+_{j+1/2}=C^{+,1}_{j+1/2}+C^{+,2}_{j+1/2}\geqslant 0$, $C^-_{j-1/2}=C^{-,1}_{j-1/2}+C^{-,2}_{j-1/2}\geqslant 0$.

Case 3: $ss_{j-1}=1$, $ss_{j+1}=-1$, Equation (12) can be expressed as

$$\begin{aligned}\frac{\mathrm{d}\bar{u}_j}{\mathrm{d}t} &= \frac{1}{h}C^{+}_{j+1/2}\delta_x^{+}\bar{u}_j - \frac{1}{h}C^{-}_{j-1/2}\delta_x^{-}\bar{u}_j \\ &= \frac{1}{2h}\left[-\frac{f(\bar{u})_{j+1}-f(\bar{u})_j}{\bar{u}_{j+1}-\bar{u}_j}+a\left(2-\frac{\bar{u}_{j+2}-\bar{u}_{j+1}}{\bar{u}_{j+1}-\bar{u}_j}\right)+4\varepsilon\frac{f(\bar{u})_{j+1}-f(\bar{u})_j}{\bar{u}_{j+1}-\bar{u}_j}\right]\delta_x^{+}\bar{u}_j \\ &\quad -\frac{1}{2h}\left[\frac{f(\bar{u})_j-f(\bar{u})_{j-1}}{\bar{u}_j-\bar{u}_{j-1}}+a\left(2-\frac{\bar{u}_{j-1}-\bar{u}_{j-2}}{\bar{u}_j-\bar{u}_{j-1}}\right)+4\varepsilon\frac{f(\bar{u})_j-f(\bar{u})_{j-1}}{\bar{u}_j-\bar{u}_{j-1}}\right]\delta_x^{-}\bar{u}_j \quad (16)\end{aligned}$$

where

$$C^{+,1}_{j+1/2}=\frac{1}{2}\left[-\frac{f(\bar{u})_{j+1}-f(\bar{u})_j}{\bar{u}_{j+1}-\bar{u}_j}+a\left(2-\frac{\bar{u}_{j+2}-\bar{u}_{j+1}}{\bar{u}_{j+1}-\bar{u}_j}\right)\right],\quad C^{+,2}_{j+1/2}=2\varepsilon\frac{f(\bar{u})_{j+1}-f(\bar{u})_j}{\bar{u}_{j+1}-\bar{u}_j}$$

$$C^{-,1}_{j-1/2}=\frac{1}{2}\left[\frac{f(\bar{u})_j-f(\bar{u})_{j-1}}{\bar{u}_j-\bar{u}_{j-1}}+a\left(2-\frac{\bar{u}_{j-1}-\bar{u}_{j-2}}{\bar{u}_j-\bar{u}_{j-1}}\right)\right],\quad C^{-,2}_{j-1/2}=2\varepsilon\frac{f(\bar{u})_j-f(\bar{u})_{j-1}}{\bar{u}_j-\bar{u}_{j-1}}$$

Obviously $C^{+,2}_{j+1/2}\geqslant 0$, $C^{-,2}_{j-1/2}\geqslant 0$.

If $\bar{u}_{j+2}-\bar{u}_{j+1}/\bar{u}_{j+1}-\bar{u}_j\leqslant 0$, $C^{+,1}_{j+1/2}\geqslant 0$.

If $\bar{u}_{j+2}-\bar{u}_{j+1}/\bar{u}_{j+1}-\bar{u}_j>0$, the condition $ss_{j+1}=\mathrm{sgn}(\delta_x^0\bar{u}_{j+1}\cdot\delta_x^2\bar{u}_{j+1})=-1$ implies $|\bar{u}_{j+2}-\bar{u}_{j+1}|<|\bar{u}_{j+1}-\bar{u}_j|$. Therefore, $\bar{u}_{j+2}-\bar{u}_{j+1}/\bar{u}_{j+1}-\bar{u}_j<1$,

$$C^{+,1}_{j+1/2}=\frac{1}{2}\left[a-\frac{f(\bar{u})_{j+1}-f(\bar{u})_j}{\bar{u}_{j+1}-\bar{u}_j}+a\left(1-\frac{\bar{u}_{j+2}-\bar{u}_{j+1}}{\bar{u}_{j+1}-\bar{u}_j}\right)\right]\geqslant 0$$

If $\bar{u}_{j-1}-\bar{u}_{j-2}/\bar{u}_j-\bar{u}_{j-1}\leqslant 0$, $C^{-,1}_{j-1/2}\geqslant 0$.

If $\bar{u}_{j-1}-\bar{u}_{j-2}/\bar{u}_j-\bar{u}_{j-1}>0$, the condition $ss_{j-1}=\mathrm{sgn}(\delta_x^0\bar{u}_{j-1}\cdot\delta_x^2\bar{u}_{j-1})=1$ implies $|\bar{u}_j-\bar{u}_{j-1}|>|\bar{u}_{j-1}-\bar{u}_{j-2}|$. Therefore, $\bar{u}_{j-1}-\bar{u}_{j-2}/\bar{u}_j-\bar{u}_{j-1}<1$,

$$C^{-,1}_{j-1/2}=\frac{1}{2}\left[a+\frac{f(\bar{u})_j-f(\bar{u})_{j-1}}{\bar{u}_j-\bar{u}_{j-1}}+a\left(1-\frac{\bar{u}_{j-1}-\bar{u}_{j-2}}{\bar{u}_j-\bar{u}_{j-1}}\right)\right]\geqslant 0$$

In this case $C^{+}_{j+1/2}=C^{+,1}_{j+1/2}+C^{+,2}_{j+1/2}\geqslant 0$, $C^{-}_{j-1/2}=C^{-,1}_{j-1/2}+C^{-,2}_{j-1/2}\geqslant 0$.

Case 4: $ss_{j-1}=-1$, $ss_{j+1}=1$, Equation (12) can be rewritten as

$$\begin{aligned}\frac{\mathrm{d}\bar{u}_j}{\mathrm{d}t} &= \frac{1}{h}C^{+}_{j+1/2}\delta_x^{+}\bar{u}_j - \frac{1}{h}C^{-}_{j-1/2}\delta_x^{-}\bar{u}_j \\ &= \frac{1}{2h}\left(-\frac{f(\bar{u})_{j+1}-f(\bar{u})_j}{\bar{u}_{j+1}-\bar{u}_j}+a+4\varepsilon\frac{f(\bar{u})_{j+1}-f(\bar{u})_j}{\bar{u}_{j+1}-\bar{u}_j}\right)\delta_x^{+}\bar{u}_j \\ &\quad -\frac{1}{2h}\left[\frac{f(\bar{u})_j-f(\bar{u})_{j-1}}{\bar{u}_j-\bar{u}_{j-1}}+a+4\varepsilon\frac{f(\bar{u})_j-f(\bar{u})_{j-1}}{\bar{u}_j-\bar{u}_{j-1}}\right]\delta_x^{-}\bar{u}_j \quad (17)\end{aligned}$$

Obviously $C^{+}_{j+1/2}\geqslant 0$, $C^{-}_{j-1/2}\geqslant 0$.

The TVDM property can be derived immediately in terms of the above results. □

For the $N \times N$ matrix A:

$$A = \begin{pmatrix} \ddots & \ddots & \ddots & 0 & 0 & 0 & 0 \\ \ddots & \ddots & \ddots & 0 & 0 & 0 & 0 \\ \ddots & \frac{1}{6}+\varepsilon & \frac{2}{3} & \frac{1}{6}-\varepsilon & 0 & 0 & 0 \\ 0 & 0 & \frac{1}{6}+\varepsilon & \frac{2}{3} & \frac{1}{6}-\varepsilon & 0 & 0 \\ 0 & 0 & 0 & \frac{1}{6}+\varepsilon & \frac{2}{3} & \frac{1}{6}-\varepsilon & \ddots \\ 0 & 0 & 0 & 0 & \ddots & \ddots & \ddots \\ 0 & 0 & 0 & 0 & \ddots & \ddots & \ddots \end{pmatrix}_{N \times N}, \quad -\frac{1}{3} < \varepsilon < \frac{1}{3} \tag{18}$$

(Strongly diagonally dominant for the transpose of A), then the L_1 norm of A^{-1} is bounded independent of N. We can prove the following facts:

1. If $-\frac{1}{3} < \varepsilon < -\frac{1}{6}$, $\|A^{-1}\|_{L_1} \leqslant 3/2(1+3\varepsilon)$.
2. If $-\frac{1}{6} \leqslant \varepsilon \leqslant \frac{1}{6}$, $\|A^{-1}\|_{L_1} \leqslant 3$.
3. If $\frac{1}{6} < \varepsilon < \frac{1}{3}$, $\|A^{-1}\|_{L_1} \leqslant 3/2(1-3\varepsilon)$.

Hence $\mathrm{TV}(u) = \sum_i |u_{i+1} - u_i| = \sum_i |A^{-1}\bar{u}_{i+1} - A^{-1}\bar{u}_i| \leqslant \|A^{-1}\|_{L_1} \sum_i |\bar{u}_{i+1} - \bar{u}_i| \leqslant \|A^{-1}\|_{L_1} \cdot \mathrm{TV}(\bar{u}^0)$.

The total variation of the numerical solution is bounded. The upwind compact approaches of the first derivative operator $(Dv)_j := \mathrm{d}v/\mathrm{d}x$ can be formulated symbolically as

$$h^{-1}\delta_x^{c,\varepsilon} := h^{-1}A^{-1}B = h^{-1}(I - 2\varepsilon\delta_x^0 + \tfrac{1}{6}\delta_x^2)^{-1}(\delta_x^0 - 2\varepsilon\delta_x^2) \tag{19}$$

where $a \cdot \varepsilon \geqslant 0$, $-\frac{1}{3} < \varepsilon < \frac{1}{3}$. If $\varepsilon \neq 0$, it achieves the third-order accuracy. If $\varepsilon = 0$, it has the fourth-order accuracy. It can be easily computed by the sweeping method.

If $\varepsilon = \pm\frac{1}{6}$, Equation (12) can be rewritten as

$$\begin{aligned} \frac{\mathrm{d}u_j}{\mathrm{d}t} = &-\frac{1}{h}\delta_x^{c,1/6}[f^+(u)_j - \varphi_j(f^+(u)_j - f^+(A_+u)_j)] + \frac{1}{2h}A_+^{-1}\delta_x^0[\varphi_j \cdot ss_j a\delta_x^2 A_+ u_j] \\ &- \frac{1}{4h}A_+^{-1}\delta_x^2[\varphi_j \cdot a\delta_x^2 A_+ u_j] - \frac{1}{h}\delta_x^{c,-1/6}[f^-(u)_j - \varphi_j(f^-(u)_j - f^-(A_-u)_j)] \\ &+ \frac{1}{2h}A_-^{-1}\delta_x^0[\varphi_j \cdot ss_j a\delta_x^2 A_- u_j] - \frac{1}{4h}A_-^{-1}\delta_x^2[\varphi_j \cdot a\delta_x^2 A_- u_j] \end{aligned} \tag{20}$$

where $f_j^{\pm} = f'^{\pm}u_j, f'^{\pm} = f' \pm |f'|/2$. The operators A_+ and A_- satisfy $A_+u_j = \frac{1}{3}u_{j-1} + \frac{2}{3}u_j$, $A_-u_j = \frac{2}{3}u_j + \frac{1}{3}u_{j+1}$, respectively.

To facilitate the calculation the above scheme can be simplified as

$$\frac{\mathrm{d}u_j}{\mathrm{d}t} = -\frac{1}{h}\,\delta_x^{c,1/6} f^+(u)_j - \frac{1}{h}\,\delta_x^{c,-1/6} f^-(u)_j + \frac{\sigma}{2h}\,\delta_x^0[\varphi_j ss_j a\delta_x^2 u_j] - \frac{\sigma}{4h}\,\delta_x^2[\varphi_j a\delta_x^2 u_j], \quad \sigma > 0 \tag{21}$$

where $\sigma \sim O(1)$, $ss_j = \mathrm{sgn}(\delta_x^0 u_j \delta_x^2 u_j)$.

The approximations for the first derivative at boundary nodes can be obtained from the given relationships. Generally speaking, the approximations are one-sides and drop to lower order accuracy. Sometimes the approximations can be obtained from the actual states of the flow fields.

4. DIFFERENCE APPROXIMATION OF THE N–S EQUATIONS

The 3D dimensionless compressible N–S equations for the perfect gas in the vector form can be expressed as

$$\frac{\partial Q}{\partial t} + \frac{\partial F_1}{\partial x} + \frac{\partial F_2}{\partial y} + \frac{\partial F_3}{\partial z} = \frac{\partial F_{v1}}{\partial x} + \frac{\partial F_{v2}}{\partial y} + \frac{\partial F_{v3}}{\partial z} \tag{22}$$

where the terms on the right-hand side are the viscous terms and F_1, F_2 and F_3 are the flux vectors corresponding to the x, y and z co-ordinate directions, respectively. Consider the N–S equations in general co-ordinate (ζ, η, ς)

$$\frac{\partial \tilde{Q}}{\partial t} + \frac{\partial \tilde{F}_1}{\partial \xi} + \frac{\partial \tilde{F}_2}{\partial \eta} + \frac{\partial \tilde{F}_3}{\partial \varsigma} = \frac{\partial \tilde{F}_{v1}}{\partial \xi} + \frac{\partial \tilde{F}_{v2}}{\partial \eta} + \frac{\partial \tilde{F}_{v3}}{\partial \varsigma} \tag{23}$$

where

$$\tilde{Q} = J^{-1}Q, \quad \tilde{F}_1 = J^{-1}[\xi_x F_1 + \xi_y F_2 + \xi_z F_3], \quad \tilde{F}_2 = J^{-1}[\eta_x F_1 + \eta_y F_2 + \eta_z F_3]$$

$$\tilde{F}_3 = J^{-1}[\varsigma_x F_1 + \varsigma_y F_2 + \varsigma_z F_3]$$

$$\tilde{F}_{v1} = J^{-1}[\xi_x F_{v1} + \xi_y F_{v2} + \xi_z F_{v3}], \quad \tilde{F}_{v2} = J^{-1}[\eta_x F_{v1} + \eta_y F_{v2} + \eta_z F_{v3}]$$

$$\tilde{F}_{v3} = J^{-1}[\varsigma_x F_{v1} + \varsigma_y F_{v2} + \varsigma_z F_{v3}]$$

$$J = 1/[x_\xi(y_\eta z_\varsigma - y_\varsigma z_\eta) - x_\eta(y_\xi z_\varsigma - y_\varsigma z_\xi) + x_\varsigma(y_\xi z_\eta - y_\eta z_\xi)]$$

The flux vector splitting technique, $\tilde{F}_l = \tilde{F}_l^+ + \tilde{F}_l^-$, $l = 1, 2, 3$, is used for the flux vectors [12]

$$\tilde{F}_l^\pm = A_l^\pm \tilde{Q}, \quad A_l^\pm = S_l^{-1}\Lambda_l^\pm S_l, \quad l = 1, 2, 3 \tag{24}$$

where A_l is the Jacobin coefficient matrix corresponding to the flux vector $\tilde{F}_l$, S_l is the matrix consisted of the left eigenvectors of the matrix A_l, $\Lambda_l^\pm$ is the diagonal matrix with elements $\lambda_l^\pm$, and $\lambda_l^\pm$ are eigenvalues of the matrix A_l.

The implicit method is used to solve this problem. Let $\Delta\tilde{Q} = \tilde{Q}^{n+1} - \tilde{Q}^n$, we have

$$\left[I + \frac{\Delta t}{2}\left(\partial_\xi A_1 + \partial_\eta A_2 + \partial_\varsigma A_3\right)\right]\Delta\tilde{Q} = \mathrm{RHS} \tag{25}$$

Jacobin coefficient matrix A_l $(l=1,2,3)$ can be split as

$$\begin{cases} \lambda(A_l^-)=V_l-c_l, & A_l^-=\lambda(A_l^-)I, & A_l^+=A_l-A_l^- \\ \lambda(A_l^-)=0 & \text{if} & V_l-c_l>0 \end{cases}, \quad l=1,2,3 \tag{26}$$

where $V_1=\xi_x u+\xi_y v+\xi_z w$, $V_2=\eta_x u+\eta_y v+\eta_z w$, $V_3=\varsigma_x u+\varsigma_y v+\varsigma_z w$ and $c_1=c\sqrt{\xi_x^2+\xi_y^2+\xi_z^2}$, $c_2=c\sqrt{\eta_x^2+\eta_y^2+\eta_z^2}$, $c_3=c\sqrt{\varsigma_x^2+\varsigma_y^2+\varsigma_z^2}$. c is the local speed of sound.

The backward difference operator is used for the matrix A_l $(l=1,2,3)$ with the positive eigenvalues, the forward difference operator is used for the matrix with the negative eigenvalues. By using the approximate factorization we have

$$\begin{cases} (I+f\delta_\xi^+A_1^-+g\delta_\eta^+A_2^-+h\delta_\varsigma^+A_3^-)\Delta\tilde{Q}^{n+1/2}=\text{RHS} \\ (I+f\delta_\xi^-A_1^++g\delta_\eta^-A_2^++h\delta_\varsigma^-A_3^+)\Delta\tilde{Q}^{n+1}=\Delta\tilde{Q}^{n+1/2} \end{cases} \tag{27}$$

where $f=\Delta t/2\Delta\xi$, $g=\Delta t/2\Delta\eta$, $h=\Delta t/2\Delta\varsigma$. The above equation can be calculated by the sweeping method. This procedure can be simplified due to the special matrix-splitting scheme. The right-hand side of the equation can be expressed as

$$\begin{aligned}
\text{RHS}&=\text{RHS}_\text{I}+\text{RHS}_\text{II}+\text{RHS}_\text{III}\\
\text{RHS}_\text{I}&=-\frac{\Delta t}{\Delta\xi}\delta_\xi^{c,1/6}\tilde{F}_{1,ijk}^+-\frac{\Delta t}{\Delta\xi}\delta_\xi^{c,-1/6}\tilde{F}_{1,ijk}^--\frac{\Delta t}{\Delta\eta}\delta_\eta^{c,1/6}\tilde{F}_{2,ijk}^+-\frac{\Delta t}{\Delta\eta}\delta_\eta^{c,-1/6}\tilde{F}_{2,ijk}^-\\
&\quad-\frac{\Delta t}{\Delta\varsigma}\delta_\varsigma^{c,1/6}\tilde{F}_{3,ijk}^+-\frac{\Delta t}{\Delta\varsigma}\delta_\varsigma^{c,-1/6}\tilde{F}_{3,ijk}^-\\
\text{RHS}_\text{II}&=\frac{\Delta t}{\Delta\xi}\delta_\xi^0\tilde{F}_{v1,ijk}+\frac{\Delta t}{\Delta\eta}\delta_\eta^0\tilde{F}_{v2,ijk}+\frac{\Delta t}{\Delta\varsigma}\delta_\varsigma^0\tilde{F}_{v3,ijk}\\
\text{RHS}_\text{III}&=\frac{\Delta t}{\Delta\xi}\sigma\delta_\xi^0[\varphi_\xi(p_{ijk})ss_\xi(p_{ijk})|\lambda_{\xi(ijk)}|\delta_\xi^2\tilde{Q}_{ijk}]-\frac{\Delta t}{2\Delta\xi}\sigma\delta_\xi^2[\varphi_\xi(p_{ijk})|\lambda_{\xi(ijk)}|\delta_\xi^2\tilde{Q}_{ijk}]\\
&\quad+\frac{\Delta t}{\Delta\eta}\sigma\delta_\eta^0[\varphi_\eta(p_{ijk})ss_\eta(p_{ijk})|\lambda_{\eta(ijk)}|\delta_\eta^2\tilde{Q}_{ijk}]-\frac{\Delta t}{2\Delta\eta}\sigma\delta_\eta^2[\varphi_\eta(p_{ijk})|\lambda_{\eta(ijk)}|\delta_\eta^2\tilde{Q}_{ijk}]\\
&\quad+\frac{\Delta t}{\Delta\varsigma}\sigma\delta_\varsigma^0[\varphi_\varsigma(p_{ijk})ss_\varsigma(p_{ijk})|\lambda_{\varsigma(ijk)}|\delta_\varsigma^2\tilde{Q}_{ijk}]-\frac{\Delta t}{2\Delta\varsigma}\sigma\delta_\varsigma^2[\varphi_\varsigma(p_{ijk})|\lambda_{\varsigma(ijk)}|\delta_\varsigma^2\tilde{Q}_{ijk}]
\end{aligned} \tag{28}$$

where $\delta_\xi^{c,\pm1/6}$, $\delta_\eta^{c,\pm1/6}$ and $\delta_\varsigma^{c,\pm1/6}$ are upwind compact difference operators and satisfy the following relations,

$$\begin{aligned}
&\tfrac{2}{3}\delta_\xi^{c,1/6}\tilde{F}_{1,ijk}^++\tfrac{1}{3}\delta_\xi^{c,1/6}\tilde{F}_{1,i-1jk}^+=\tfrac{1}{6}\tilde{F}_{1,i+1jk}^++\tfrac{2}{3}\tilde{F}_{1,ijk}^+-\tfrac{5}{6}\tilde{F}_{1,i-1jk}^+,\\
&\tfrac{1}{3}\delta_\xi^{c,-1/6}\tilde{F}_{1,i+1jk}^-+\tfrac{2}{3}\delta_\xi^{c,-1/6}\tilde{F}_{1,ijk}^-=\tfrac{5}{6}\tilde{F}_{1,i+1jk}^--\tfrac{2}{3}\tilde{F}_{1,ijk}^--\tfrac{1}{6}\tilde{F}_{1,i-1jk}^-
\end{aligned} \quad (i=1,2,\ldots,I-1) \tag{29a}$$

$$\begin{aligned}
&\tfrac{2}{3}\delta_\eta^{c,1/6}\tilde{F}^+_{2,ijk} + \tfrac{1}{3}\delta_\eta^{c,1/6}\tilde{F}^+_{2,ij-1k} = \tfrac{1}{6}\tilde{F}^+_{2,ij+1k} + \tfrac{2}{3}\tilde{F}^+_{2,ijk} - \tfrac{5}{6}\tilde{F}^+_{2,ij-1k},\\
&\tfrac{1}{3}\delta_\eta^{c,-1/6}\tilde{F}^-_{2,ij+1k} + \tfrac{2}{3}\delta_\eta^{c,-1/6}\tilde{F}^-_{2,ijk} = \tfrac{5}{6}\tilde{F}^-_{2,ij+1k} - \tfrac{2}{3}\tilde{F}^-_{2,ijk} - \tfrac{1}{6}\tilde{F}^-_{2,ij-1k}
\end{aligned} \qquad (j = 1,2,\ldots,J-1) \tag{29b}$$

$$\begin{aligned}
&\tfrac{2}{3}\delta_\varsigma^{c,1/6}\tilde{F}^+_{3,ijk} + \tfrac{1}{3}\delta_\varsigma^{c,1/6}\tilde{F}^+_{3,ijk-1} = \tfrac{1}{6}\tilde{F}^+_{3,ijk+1} + \tfrac{2}{3}\tilde{F}^+_{3,ijk} - \tfrac{5}{6}\tilde{F}^+_{3,ijk-1},\\
&\tfrac{1}{3}\delta_\varsigma^{c,-1/6}\tilde{F}^-_{3,ijk+1} + \tfrac{2}{3}\delta_\varsigma^{c,-1/6}\tilde{F}^-_{3,ijk} = \tfrac{5}{6}\tilde{F}^-_{3,ijk+1} - \tfrac{2}{3}\tilde{F}^-_{3,ijk} - \tfrac{1}{6}\tilde{F}^-_{3,ijk-1}
\end{aligned} \qquad (k = 1,2,\ldots,K-1) \tag{29c}$$

At the boundary points the second-order accurate one-side difference approximations are used

$$\begin{aligned}
\delta_\xi^{c,1/6}\tilde{F}^+_{1,0jk} &= (-3\tilde{F}^+_{1,0jk} + 4\tilde{F}^+_{1,1jk} - \tilde{F}^+_{1,2jk})/2\\
\delta_\xi^{c,-1/6}\tilde{F}^-_{1,Ijk} &= (3\tilde{F}^-_{1,Ijk} - 4\tilde{F}^-_{1,I-1jk} + \tilde{F}^-_{1,I-2jk})/2\\
\delta_\eta^{c,1/6}\tilde{F}^+_{2,i0k} &= (-3\tilde{F}^+_{2,i0k} + 4\tilde{F}^+_{2,i1k} - \tilde{F}^+_{2,i2k})/2\\
\delta_\eta^{c,-1/6}\tilde{F}^-_{2,iJk} &= (3\tilde{F}^-_{2,iJk} - 4\tilde{F}^-_{2,iJ-1k} + \tilde{F}^-_{2,iJ-2k})/2\\
\delta_\varsigma^{c,1/6}\tilde{F}^+_{3,ij0} &= (-3\tilde{F}^+_{3,ij0} + 4\tilde{F}^+_{3,ij1} - \tilde{F}^+_{3,ij2})/2\\
\delta_\varsigma^{c,-1/6}\tilde{F}^-_{3,ijK} &= (3\tilde{F}^-_{3,ijK} - 4\tilde{F}^-_{3,ijK-1} + \tilde{F}^-_{3,ijK-2})/2
\end{aligned} \tag{30}$$

$\delta_\xi^{c,\pm1/6}\tilde{F}^\pm_{1,ijk}$, $\delta_\eta^{c,\pm1/6}\tilde{F}^\pm_{2,ijk}$ and $\delta_\varsigma^{c,\pm1/6}\tilde{F}^\pm_{3,ijk}$ can be obtained by the alternating direction sweeping method.

$\varphi_\xi(p_{ijk})$, $\varphi_\eta(p_{ijk})$ and $\varphi_\varsigma(p_{ijk})$ are switch functions, which are similar to formula (11). They can guarantee that the obtained scheme is $O(h^3)$ in smooth regions and the group velocity of wave packets can be controlled near the shocks. $ss_\xi(p_{ijk}) = \mathrm{sgn}(\delta_\xi^2 p_{ijk} \cdot \delta_\xi^0 p_{ijk})$, $ss_\eta(p_{ijk}) = \mathrm{sgn}(\delta_\eta^2 p_{ijk} \cdot \delta_\eta^0 p_{ijk})$ and $ss_\varsigma(p_{ijk}) = \mathrm{sgn}(\delta_\varsigma^2 p_{ijk} \cdot \delta_\varsigma^0 p_{ijk})$. $\lambda_{\xi(ijk)}$, $\lambda_{\eta(ijk)}$ and $\lambda_{\varsigma(ijk)}$ are the maximum eigenvalues of A_l $(l = 1,2,3)$. p_{ijk} denotes the local pressure at node (i,j,k), $\sigma \sim O(1)$.

5. NUMERICAL EXAMPLES FOR MODEL EQUATIONS

To test the behaviour of the method, we consider the following examples.

Example 1

Pulses, wave packets and wave fronts.

In order to test the central compact difference operator is a slow operator we compute a pulses. For a direct observation of group velocity, it is simplest to look at a wave packet as in Figure 1. The region shown is the interval $[0, 10]$, on which a mesh of size $h = 0.025$ has been placed. The initial packet is several sine waves modulated by a Gaussian centred at $x = 0.5$, with the different wave-numbers,

$$u(x,0) = \mathrm{e}^{-16(x-0.5)^2}(\sin 10\pi x + \sin 20\pi x + \sin 30\pi x)$$

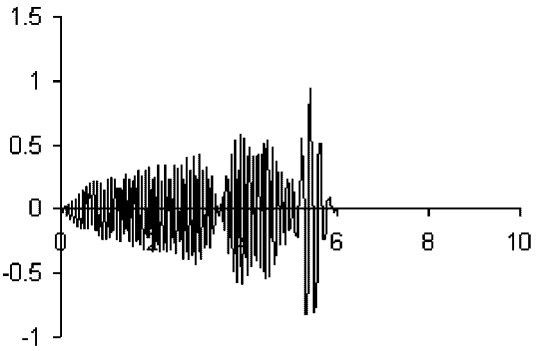

Figure 1. Propagation of wave packets with different wave numbers (5, 10, 15) under $u_t + u_x = 0$.

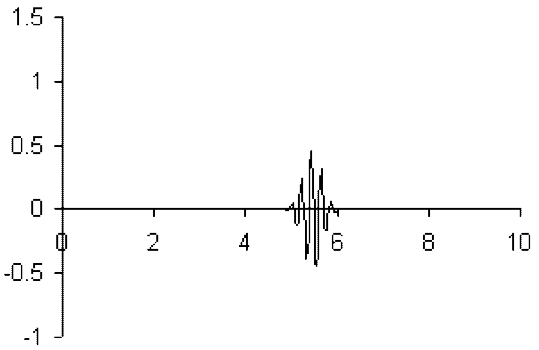

Figure 2. Propagation of wave packets with $\varepsilon = 0.05$.

The fourth-order accurate central compact difference operator is employed. The third-order $R-K$ time discretization is employed. In order to reduce the effects of the time discretization, the CFL number is small. Here $\Delta t/\Delta x = 0.01$. Figure 1 shows that the numerical solutions at the time $t = 5$. We can see that the wave packets move not at the ideal velocity 1, the centre of the group of waves is not at $x = 5.5$. The central compact difference operator is a slow operator.

Higher wave numbers have lower group velocity and lag behind this position, the low wave numbers travel at velocity nearly 1, as they must. The dispersion of the waves occurs. Figure 2 shows the numerical results with $\varepsilon = 0.05$. We can see that the higher wave numbers have been damped due to diffusion.

Example 2

The propagation of discontinuity.

Consider the following equation:

$$\frac{\partial u}{\partial t} + \frac{\partial u}{\partial x} = 0$$

The initial condition is $u(x,0) = \begin{cases} 1, & x \leqslant \frac{1}{3} \\ 0, & x > \frac{1}{3}. \end{cases}$

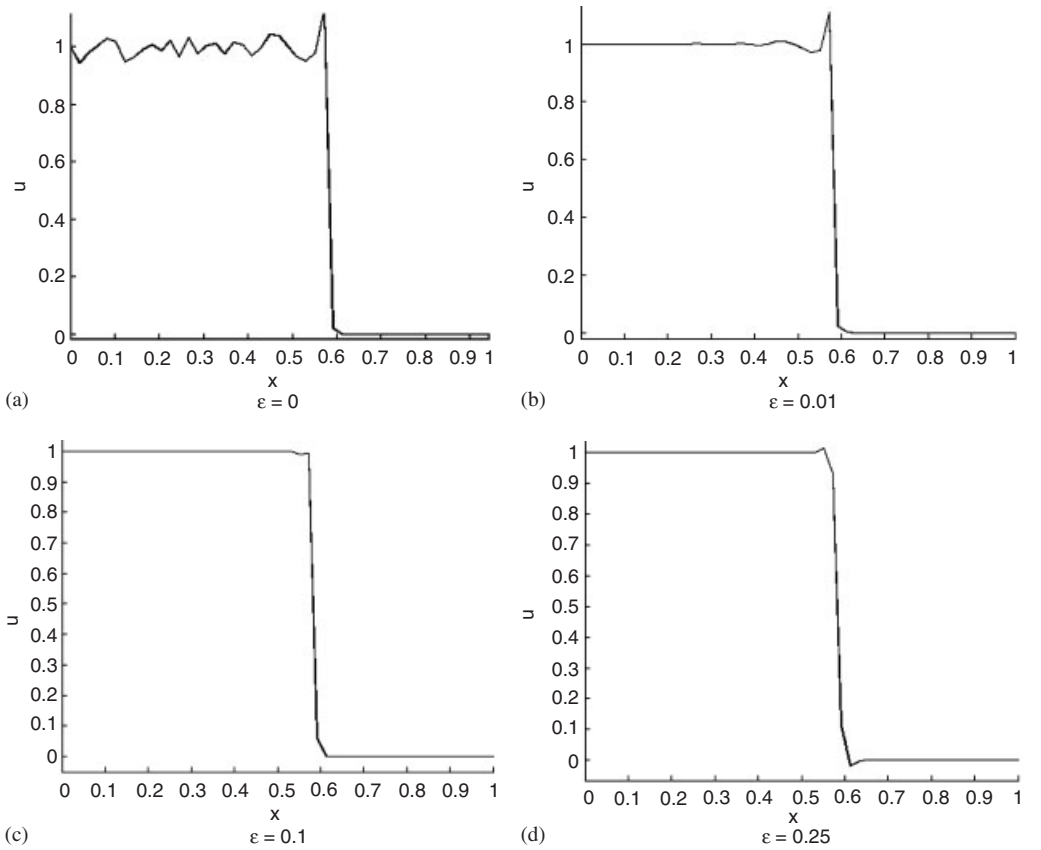

Figure 3. Numerical solutions of Example 2.

We will test the upwind compact method with group velocity control. We have known that the TV of this scheme is bounded in the semi-discrete form. Under the appropriate restriction on the time step this method satisfies the TVB property.

Here $\Delta t/\Delta x = 0.1$. and $\mathrm{IN} = 201$, $0 \leqslant x \leqslant 1$. Figure 3 shows that the numerical solutions at $t = 500\Delta t$ with different ε, $(\varepsilon = 0, \varepsilon = 0.01, \varepsilon = 0.1, \varepsilon = 0.25)$, respectively.

We can see that the oscillations occur behind the discontinuity with small ε. The numerical oscillations will happen in front of the discontinuity as ε increases. Here the solution function consists of the waves with different wave numbers. When $\varepsilon = 0$, the compact operator is a slow operator. The group velocity $\mathrm{d}\,\mathrm{Im}[\hat{\delta}_x^c(\xi)]/\mathrm{d}\xi \leqslant 1$, $\forall|\xi| \leqslant \pi$, the propagation of the wave packets is slower than the velocity 1. The dispersion of the waves occurs behind the discontinuity. With the increment of ε the upwind compact operator becomes the mixed operator. The oscillations will occur between the two sides of the discontinuity. Here Figures 3(a)–(c) show that the oscillations occur behind the discontinuity. Figure 3(d) shows that some spurious oscillations occur between the two sides of the discontinuity. Figure 4 shows the numerical solutions of the equation by using UCGVC3. The numerical oscillations are suppressed. The result is satisfactory.

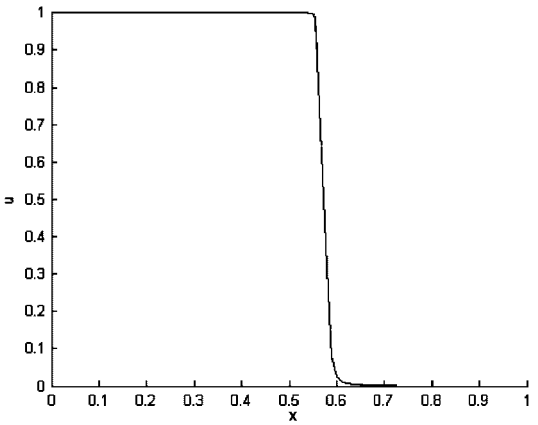

Figure 4. Numerical solutions with UCGVC3.

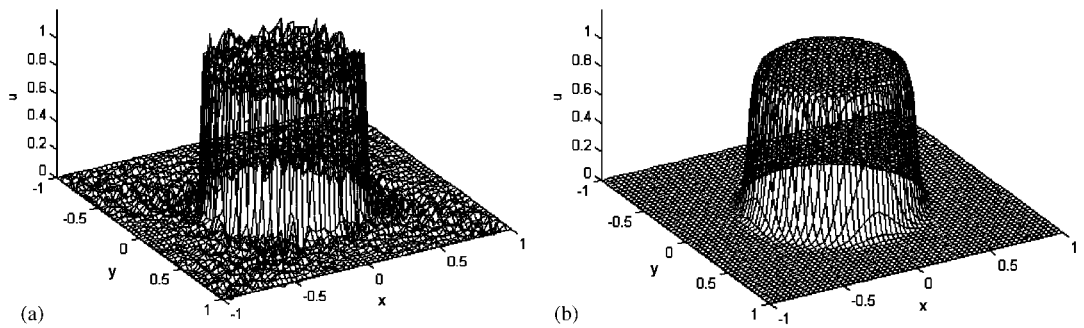

Figure 5.

Example 3

Consider the following two-dimensional linear conservation law with variable coefficients:

$$u_t + (-yu)_x + (xu)_y = 0, \quad -1 \leqslant x, y \leqslant 1$$

with periodic boundary conditions. The initial condition is chosen as the characteristic function of a circle of radius 0.5. The governing equation denotes a solid body rotation. The results at $t = 2$, using 200×200 points, is shown in Figure 5(b). Figure 5(a) shows that numerical oscillations occur in the vicinity of the discontinuity when the group velocity is not controlled. By using UCGVC3 we derive a satisfactory result. The numerical oscillations have been eliminated.

6. NUMERICAL SIMULATIONS OF COMPRESSIBLE FLOW FIELDS

6.1. Heat transfer problems

6.1.1. Boundary conditions. In order to demonstrate the performance of UCGVC3 we simulate the compressible flow fields around a sphere. The non-skip condition is used on the

Table I.

Method	Mesh Reynolds number	Numerical solutions	Fay–Riddell's estimates [13]
UCGVC3	12.46	3.51×10^{-3}	3.83×10^{-3}
	9.56	3.63×10^{-3}	
	7.15	3.73×10^{-3}	
	4.58	3.83×10^{-3}	
TVD	12.46	1.70×10^{-3}	
	9.56	2.20×10^{-3}	
	7.15	2.68×10^{-3}	
	4.58	3.15×10^{-3}	

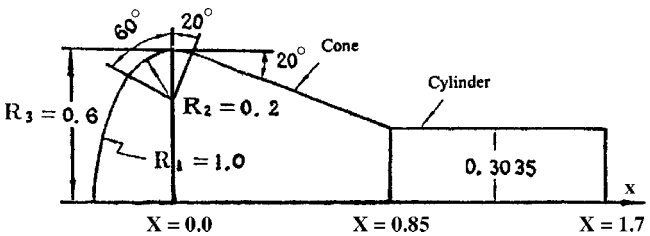

Figure 6. Geometric shape of re-entry vehicle.

surface of the sphere. The free stream conditions are used at the inflow boundary. ρ, ρu, ρv, ρw, e at the outflow are obtained from extrapolation of the interior nodes.

6.1.2. Numerical results and discussions. We simulated the flow fields around a sphere and calculated the heat transfer at the stagnation point by UCGVC3. The inflow conditions are: $M_\infty = 7.0$, $Re_\infty = 1.48 \times 10^5$, $T_\infty = 67$ K, $T_w = 300$ K. The grid system with 19×31 is employed in the present computation. Table I shows the numerical solutions obtained by UCGVC3 and TVD in the same grid system. Compared with the TVD scheme, UCGVC3 can be used to obtain the better numerical solutions at the higher mesh Reynolds number.

6.2. 3D Compressible flow fields around re-entry vehicle

6.2.1. Boundary conditions. In order to demonstrate the performance of UCGVC3 we simulate the 3D complex compressible flow fields around re-entry vehicles. The non-skip condition is used on the surface of the spaceship. The circumferential mean values around the symmetrical axis are used. The symmetrical conditions are employed in the symmetrical plane. The free stream conditions are used at the inflow boundary. ρ, ρu, ρv, ρw, e at the outflow are obtained from extrapolation of the interior nodes.

6.2.2. Numerical results and discussions. The 3D viscous flow fields around re-entry vehicles are very complicated. The shocks and three-dimensional multi-scale separations exist in such flow fields. The aerodynamic heating also occurs on its surface. In order to capture the shocks and the vortices with small scales, meanwhile, improve the stability of the difference scheme we use UCGVC3 to simulate the 3D flow fields. The shape of the re-entry vehicle is shown in Figure 6. It consists of two parts. Fore-body and after-body, which are cone

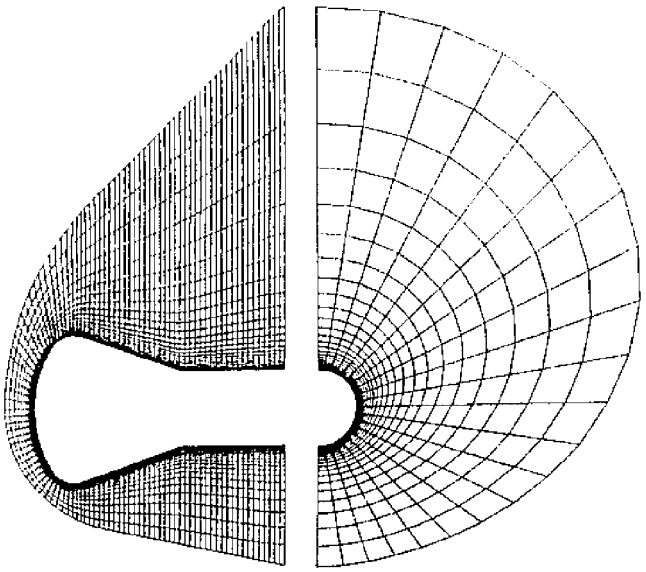

Figure 7. Grid system.

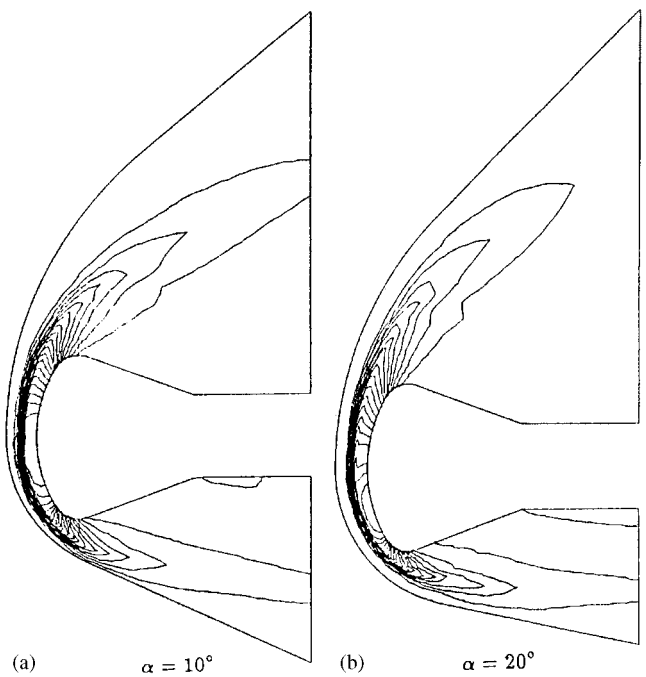

Figure 8. Pressure contours in the symmetrical plane.

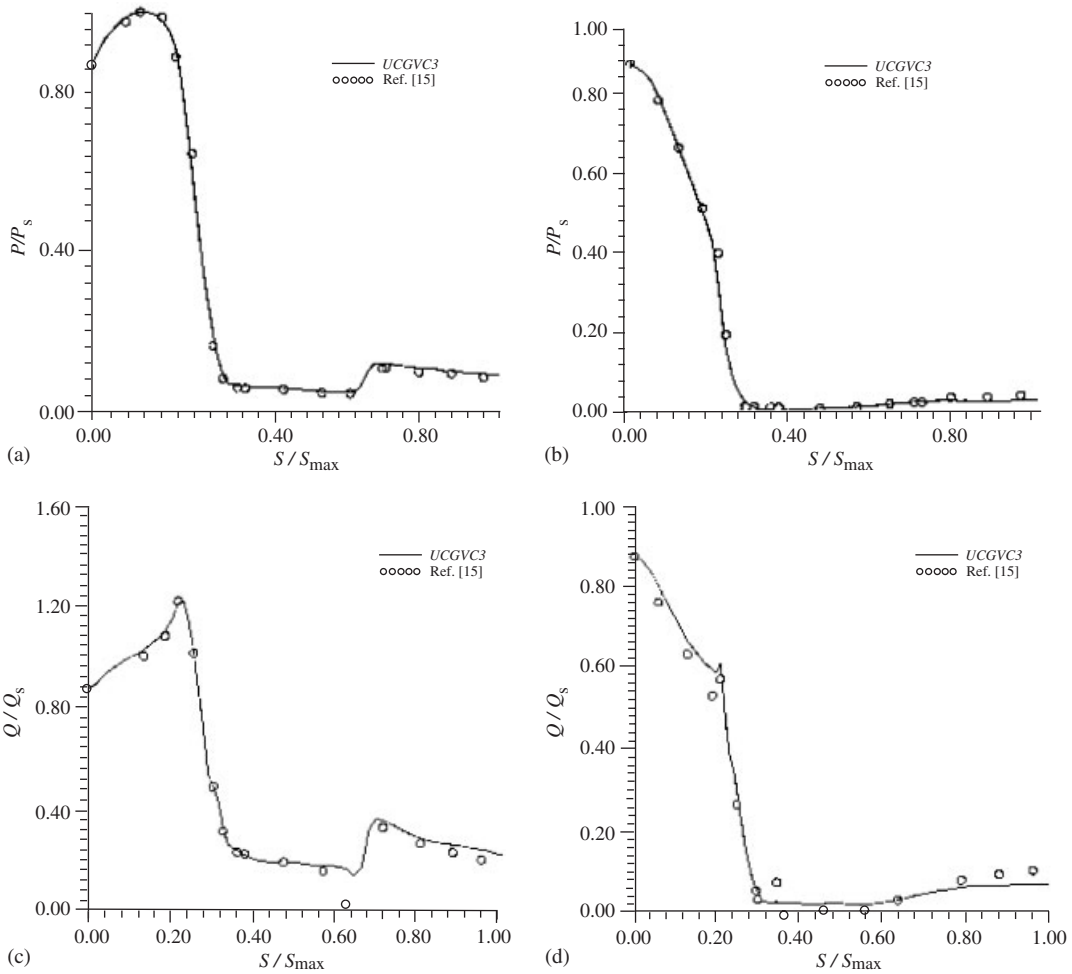

Figure 9. (a) Pressure distribution on the upwind surface ($\alpha = 20^\circ$). (b) Pressure distribution on the lee-wind surface ($\alpha = 20^\circ$). (c) Heat flux distribution on the upwind surface ($\alpha = 20^\circ$). (d) Heat flux distribution on the lee-wind surface ($\alpha = 20^\circ$).

and cylinder, respectively. The inflow conditions are: $M_\infty = 7.0$, $Re_\infty = 4.5 \times 10^5$, $T_\infty = 67\,\mathrm{K}$, $T_w = 300\,\mathrm{K}$.

The grid system with $62 \times 41 \times 21$ is employed in the present computation, as shown in Figure 7. For comparison we also use TVD to simulate the 3D flow fields. The same grid system is used. Due to simulation of the viscous flow fields the mesh near the surface of the re-entry vehicle is refined. Figure 8 shows the pressure contours in the symmetrical plane. The angles of attack are 10 and 20°, respectively. Q_0 denotes the heat flux at the stagnation point at the angle of attack 0°. $Q_0 = 3.94 \times 10^{-3}$, which is close to the Fay–Riddell's estimates. Due to the discontinuity of the curvature at the shoulder of the re-entry vehicle a peak of heat flux appears at the shoulder of the vehicle. The amplitude of the peak increases with the

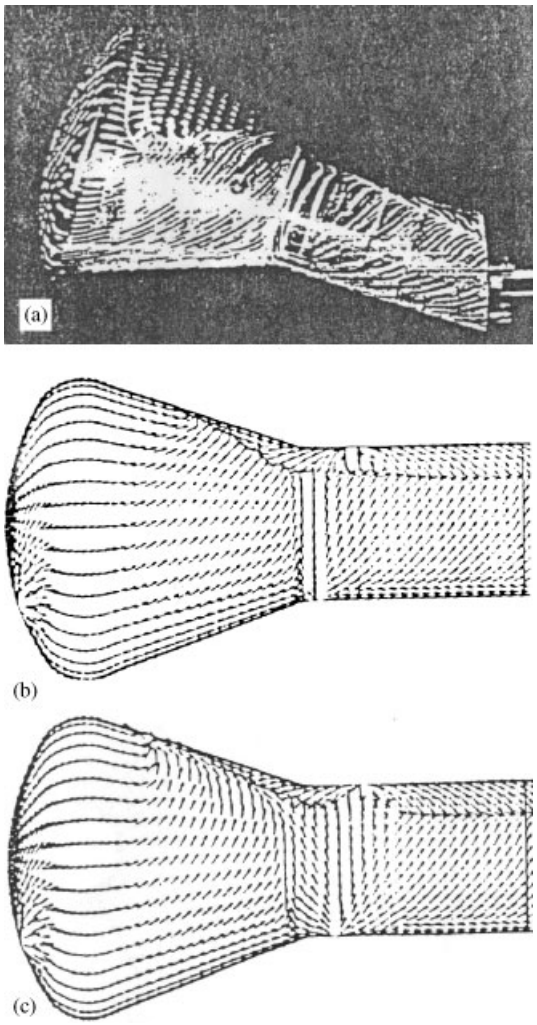

Figure 10. (a) Experimental friction curves on the surface ($\alpha = 20^\circ$). (b) Friction curves on the surface (TVD) ($\alpha = 20^\circ$). (c) Friction curves on the surface (UCGVC3) ($\alpha = 20^\circ$).

increment of the curvature of the shoulder. It agrees well with the experiment by Shih [14]. Figure 9 shows the distribution of the pressure and heat flux on the surface of the vehicle. It has agreement with the results in Reference [15]. S denotes the arc length. $S = 0$ and $S_{\max}$ correspond to the apex of the vehicle and export, respectively. P_s denotes the pressure at the stagnation point. Q_s denotes the heat flux at the stagnation point. When the angle of attack is 10°, $Q_p/Q_{0\alpha=0^\circ} = 1.21$; the angle of attack is 20°, $Q_p/Q_{0\alpha=0^\circ} = 1.36$, where Q_p denotes the peak of the heat flux. Figure 10(c) shows the friction curves on the surface of the vehicle at the angle of attack 20°, obtained by UCGVC3. For comparison, Figure 10(a) and (b) show the experimental results and computational results by TVD, respectively. The tornado on the

lee-wind surface of the cone has been clearly simulated. However, it is not obvious by the TVD method. This is because of the over-dissipative effects of the TVD method.

7. CONCLUSIONS

In this paper we are interested in investigating an upwind compact difference scheme with group velocity control, calculating the compressible flow fields. The purpose of the paper is to consider the applicability of the newly developed method for capturing the shock and the small structures in the compressible complex flow fields. Compared with the central compact finite difference scheme, the upwind compact finite difference scheme is an upwind-biased scheme, which is better for simulation of the 3D compressible flow fields due to stability. We have proved that UCGVC3 satisfies TVB property. This scheme is used to simulate the 3D compressible flow fields around a spaceship. It is useful for both capturing the shocks and the vortices.

ACKNOWLEDGEMENTS

We would like to thank the National Natural Science Foundation of China under Grant 10102024 and the Hong Kong Polytechnic University for funding this research.

REFERENCES

1. Dexun Fu, Yanwen Ma. High resolution schemes. In *Computational Fluid Dynamics Review*, Hefez M, Oshima K (eds). Wiley: Chichester, 1995; 234–250.
2. Leonard BP. A stable and accurate convective modeling procedure based on quadratic upstream interpolation. *Computer Methods in Applied Mechanics and Engineering* 1979; **19**:59–98.
3. Rai MM, Moin P. Direct simulation of turbulent flow using finite difference schemes. *Journal of Computational Physics* 1991; **96**(1):15–53.
4. Dexun Fu, Yanwen Ma. A high order accurate finite difference scheme for complex flow fields. *Journal of Computational Physics* 1997; **134**:1–15.
5. Lele SK. Compact finite difference schemes with spectral-like resolution. *Journal of Computational Physics* 1992; **103**:16–42.
6. Weinan E, Jian-Guo Liu. Essentially compact schemes for unsteady viscous incompressible flows. *Journal of Computational Physics* 1996; **126**(1):122–138.
7. Qingyong Zhu, Yanwen Ma. A high order accurate upwind compact finite difference scheme with group velocity control for solving hyperbolic conservation laws. *Chinese Journal of Computational Physics* 1998; **15**(5): 531–536.
8. Peter C Chu, Chenwu Fan. A three-point combined compact difference scheme. *Journal of Computational Physics* 1998; **140**(2):370–399.
9. Yabe T, Xiao F, Utsumi T. The constrained interpolation profile method for multiphase analysis. *Journal of Computational Physics* 2001; **169**(2):556–593.
10. Dexun Fu, Yanwen Ma. Non-physical oscillations in numerical solutions—reason and improvement. *Computational Fluid Dynamics Journal* 1995; **4**(4):427–450.
11. Swanson RC. On central-difference and upwind schemes. *Journal of Computational Physics* 1992; **101**: 292–306.
12. Steger JL, Warming RF. Flux vector splitting of the in viscid gasdynamic equations with application to finite difference methods. *Journal of Computational Physics* 1981; **40**:263–293.
13. Fay JA, Riddell RF. Theory of stagnation point heat transfer in dissociated air. *Journal of Aeronautical Sciences* 1958; **25**:73–85.
14. Shih PK, Gay A. Low L/D aerobrake heat transfer test at Mach 10. *AIAA Paper*, 1984; 984-309.
15. Yamamoto Y. Numerical simulation of hypersonic viscous fore- and after-body flows over capsule-type vehicles at angles of attack. *AIAA Paper*, 1985; 85-0924.

